Roughness evaluation on a splay of the active fault system responsible of the massive 2016 seismic sequence of Central Apennines (Italy)

Amerigo Corradetti[1]*, Stefano Tavani[2], Miller Zambrano[3], Emanuele Tondi[3], and Thomas Daniel Seers[1]

[1]Texas A&M University at Qatar, Doha, Qatar (*amerigo.corradetti@qatar.tamu.edu)
[2]Università di Napoli Federico II, Naples, Italy
[3]Università di Camerino, Camerino, Italy

EGU2020-10636
https://doi.org/10.5194/egusphere-egu2020-10636
EGU General Assembly 2020

The roughness of seismogenic faults is a key element for understanding the seismic cycle.

Earthquakes nucleate at depths that are not physically accessible, so that fault roughness profiles or maps are generally derived along active Earth's ruptures at surface and typically used as analogue of the roughness representative of seismogenic conditions.

Here, we present a study conducted on a splay of the Mt. Vettore fault system in the central Apennines (Italy), after a major seismic crisis exposed new portions of the fault in 2016. We have made a highly detailed model of a section of the fault using SfM photogrammetry, to assess its roughness parameters (i.e. the Hurst fractal parameter) and to determine the extent to which these parameters are affected by weathering.

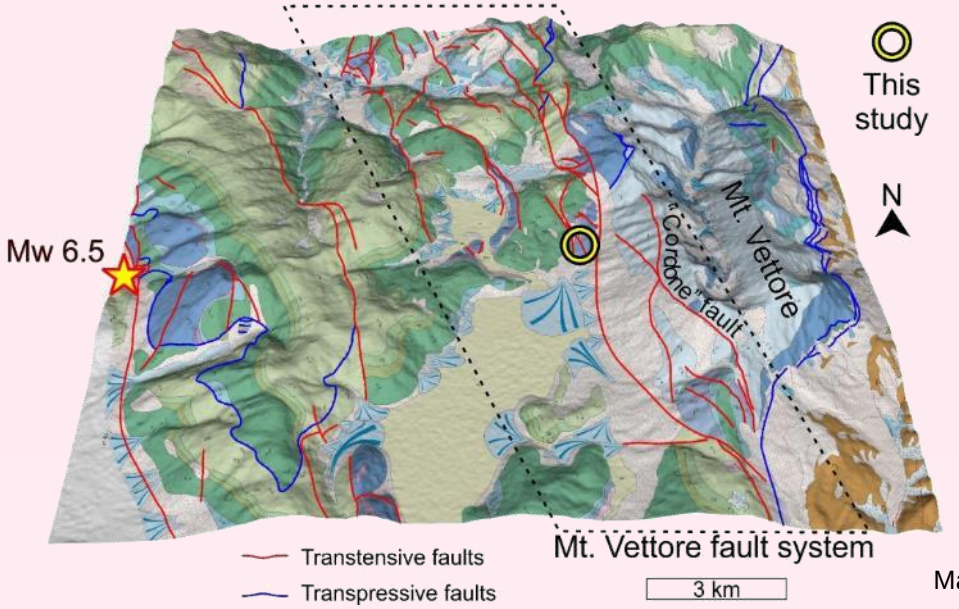

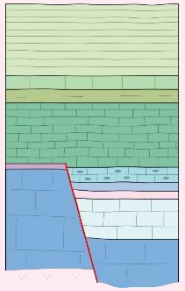

Map from Pierantoni et al. (2013), modified and draped over a DEM.

Data acquisition

Photograph of the studied fault with the location of the reconstructed model and the ruler used for scaling the model. Four zones (i.e. bands) with different aspect and color can be recognized. The direction of the wear striations (i.e. slip direction) and the slope direction (surface runoff-driven erosion) are also indicated by the blue and the green arrows, respectively.

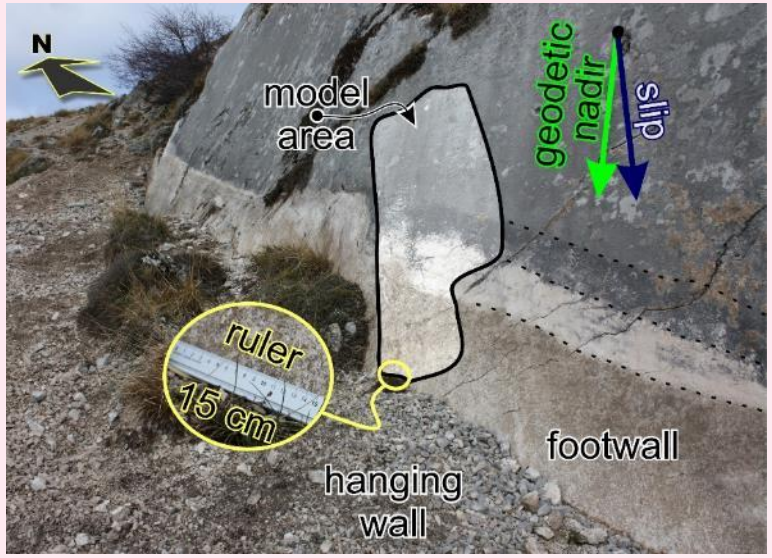

Fault topography acquisition workflow:

- Field equipment consisted of a tripod, a camera, and a ruler for scale.
- The model was built in Agisoft PhotoScan. The position of the photographs and of the scale is indicated. A dense point cloud of about 250 million points was constructed.

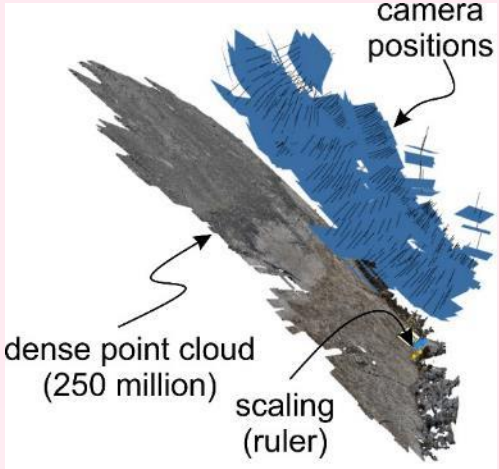

Method described in Corradetti et al. (2017)

(Left) The resulting model is a point cloud of 250 million of vertexes.
(Center) Distance distribution (calculated in CloudCompare) from a plane of best fit and the point cloud.
(Right) The main surface was divided into 315 sub-areas and analyzed independently.

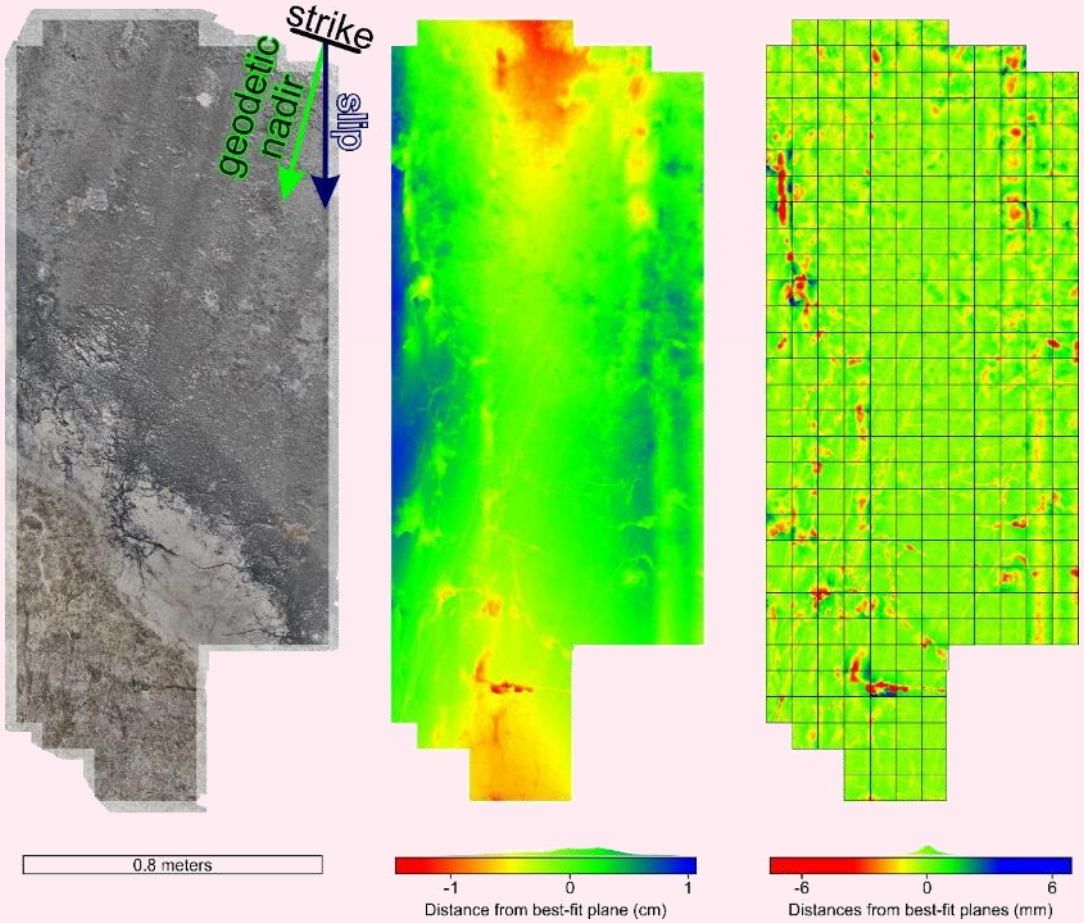

Roughness evaluation

Fault roughness of each sub-area was characterized by the standard deviation of the residual distances from its plane of best fit, and by an evaluation of self-affinity using a Fourier Power Spectral Density (PSD / Schuster, 1898) approach. These two indicators together can fully define fracture roughness (e.g. Brown, 1995).

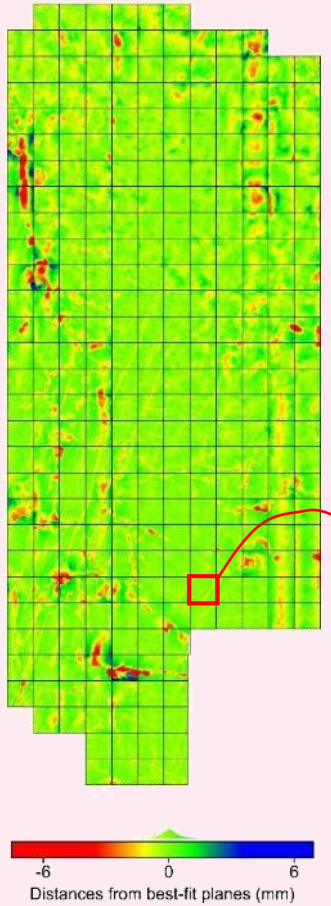

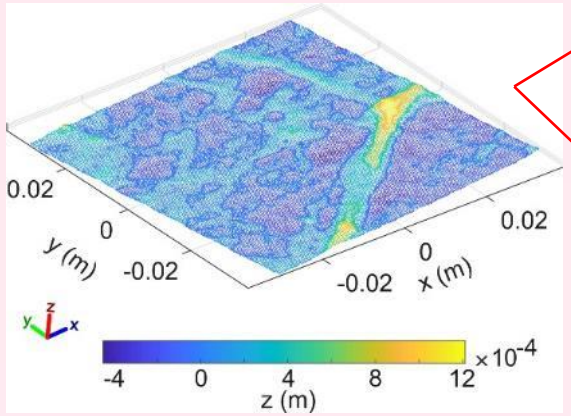

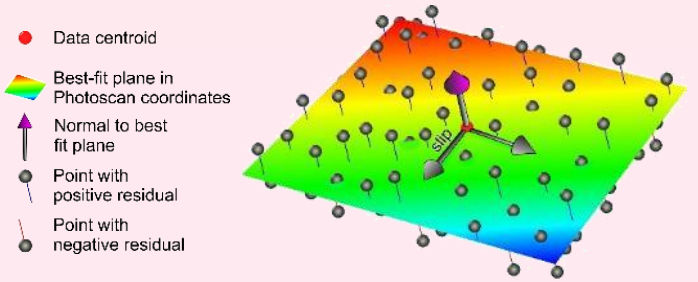

Standard deviation is one of the most commonly used metrics to describe deviation from the plane of best fit (i.e. residual distances or error).

The **PSD** as a function of the wavenumber (k) in a bi-logarithmic scale graph of a self-affine function exhibits an apparent linear slope, which is defined from the following power law

$P(k) = \alpha \cdot k^{-\beta}$ (Eq. 1)

where α is the pre-factor and the β is the exponent of the power-law.
This latter parameter (β) is related to the scaling exponent or Hurst exponent (H) along the direction of the analyzed signal through:

$H = (\beta - 1)/2$ (Eq. 2)

The self-affinity of a fault is thus defined by the ratio of the Hurst exponent and of the pre-factor calculated perpendicular and parallel to slip (i.e. H_{perp}/H_{slip} and $\alpha_{perp}/\alpha_{slip}$).

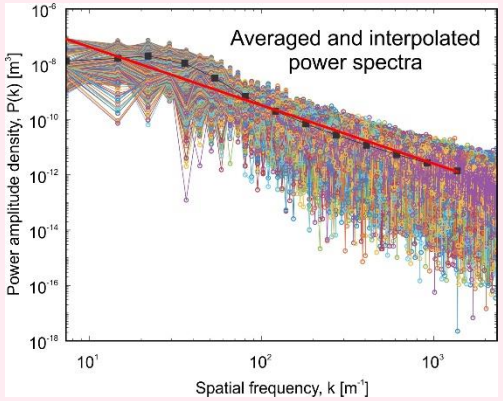

The Fast Fourier Transform (FFT) analysis of each resampled surface was achieved using a 1D FFT approach (e.g. Renard et al., 2013).
All power spectra associated with each direction of each sub-area (i.e. parallel or perpendicular to slip) were stacked and averaged in a geometric progression with a regularly spaced frequency (k). Averaging in geometric progression allowed the computation of the best fit of the form of Eq. 1 that is not biased by a differential in the frequency of shorter and longer wavelengths.

Results (1/2)

After analyzing each sub-area independently, we have grouped the results in 4 zones.

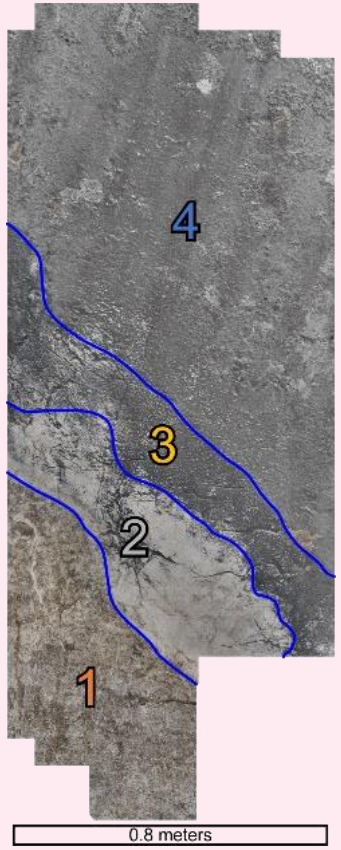

Zones 1 and 2 show a whitish colored cataclastic slickenside. Zone 1 was freshly exposed and contaminated with soil at the time of the acquisition. The smooth cataclastic slickenside is preserved as small patches within the Zone 3, while weathering has completely removed it from Zone 4.

SVD results.
(Above) Normalized frequency distribution histogram of the standard deviation of the residuals for all the 315 sub-models plotted in bins of 0,2 mm each. Dashed lines are 1000 (normally) randomly generated values generated using the mean and the standard deviation of each population
(Below) Cumulative distribution of the standard deviation of residuals displayed semi-logarithmically.

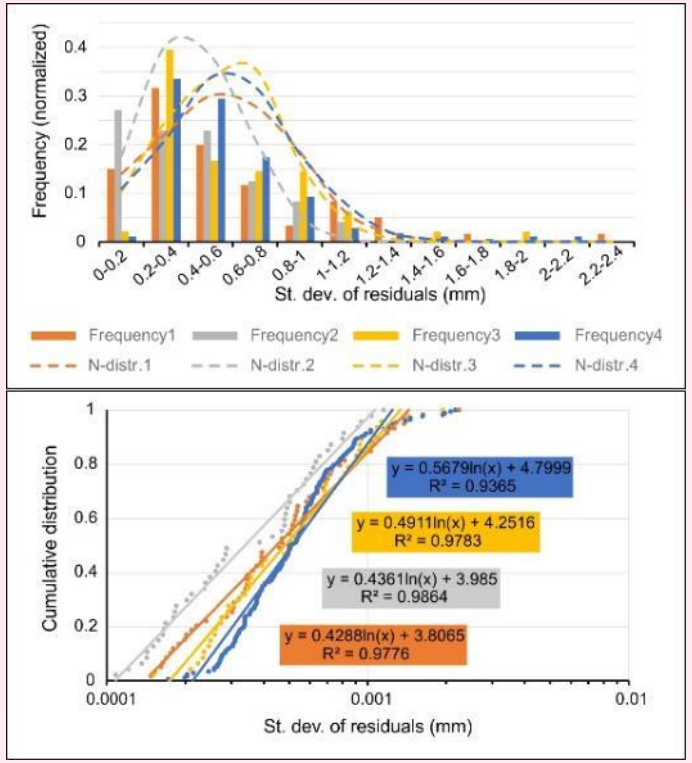

SVD results filtered of fractured sub-areas showing the highest densities of large open fractures.
(Above) Normalized frequency distribution histogram of the standard deviation of the residuals for the filtered sub-models plotted in bins of 0,1 mm each.
(Below) Cumulative distribution of the standard deviation of residuals displayed semi-logarithmically.

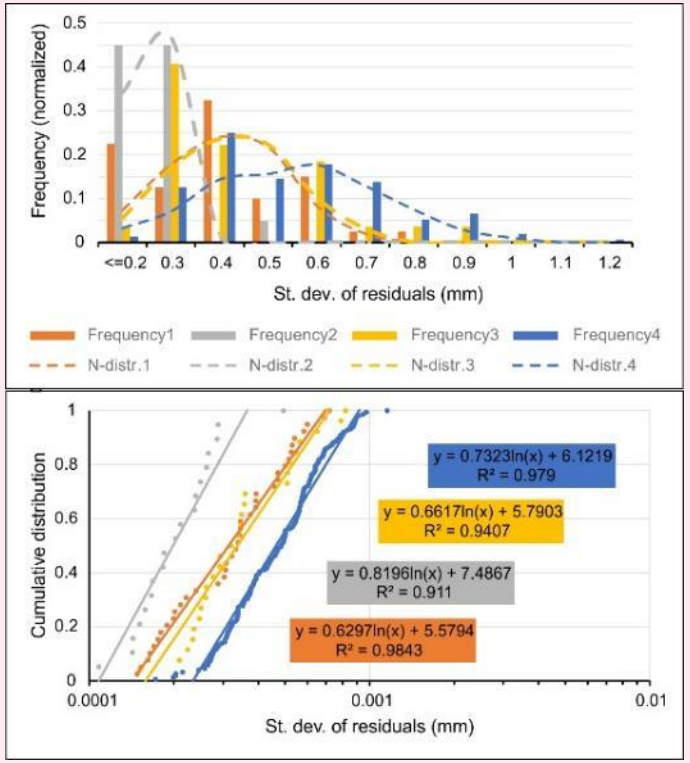

Results (2/2)

Normalized frequency distributions of the Hurst exponents along the direction of slip (left) and perpendicularly to it (right).
Dashed lines represent the normal distributions over 1000 randomly generated numbers using the mean and the standard deviation of each population described before.

Normalized frequency distributions of the pre-factor along the direction of slip (left) and perpendicularly to it (right).

Frequency distribution of the Hurst exponents (left) and pre-factors (right) ratio calculated between the perpendicular to slip direction over those aligned to the slip direction.

PSD results filtered of fractured sub-areas.

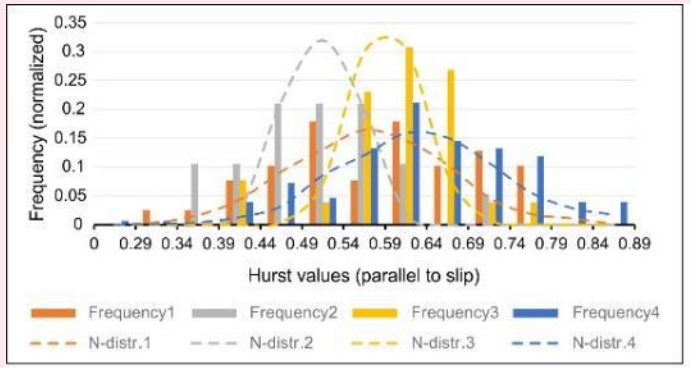

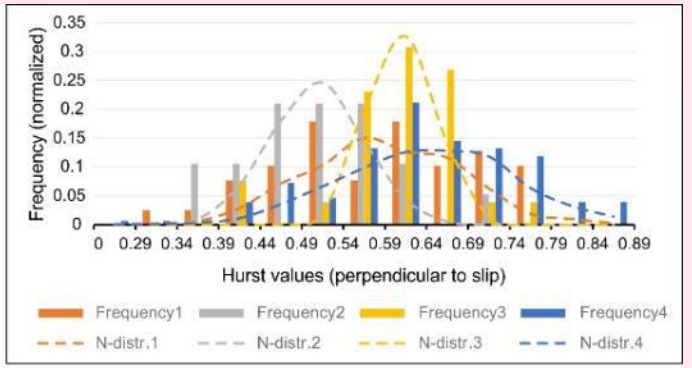

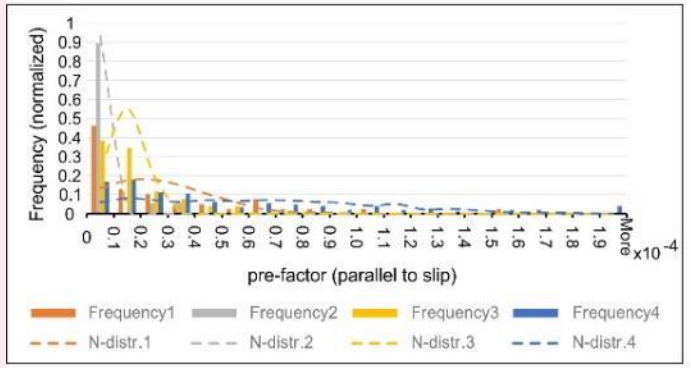

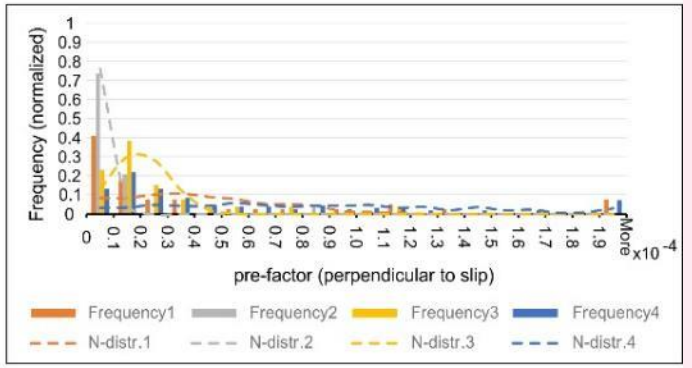

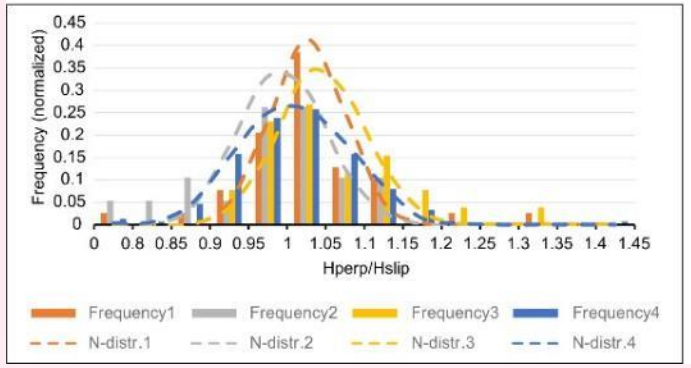

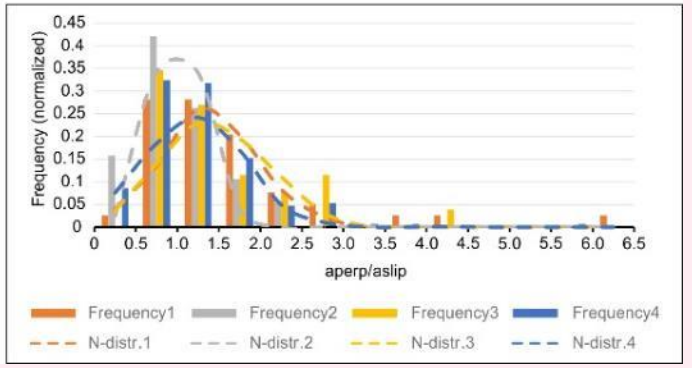

Conclusions

SfM-MSV photogrammetry has been used here to generate a highly detailed point cloud of an active carbonate fault within the Mt. Vettore fault system (Italy).

We have estimated and compared the fault roughness of patches of fault exposed to weathering over different timescales by means of the standard deviation of the surfaces' residual distances and by measures of self-affinity.

The fault studied in this work is likely quite isotropic in origin as shown by the clustering around 1 of both H_{perp}/H_{slip} and a_{perp}/a_{slip} for Zone 2 (which is the least weathered and most recently uncovered zone).

Results show that weathering modify the value of the fractal parameters. In particular, by independently analyzing different patches of the fault, we have observed that the smoother and recently exposed portions of the fault have lower values of Hurst exponent and pre-factor.

In conclusion we have evidenced that even with active normal faults that are generally considered to represent the best available targets to study seismogenic roughness at macro to mesoscales, caution must be paid to the relative exposure time of the faulted outcrop analogue.

References

BROWN, S.R. 1995. Simple mathematical model of a rough fracture. *Journal of Geophysical Research: Solid Earth* **100**(B4), 5941–5952.

CORRADETTI, A., MCCAFFREY, K.J.W., DE PAOLA, N. & **TAVANI, S.** 2017. Evaluating roughness scaling properties of natural active fault surfaces by means of multi-view photogrammetry. *Tectonophysics* **717**, 599–606.

PIERANTONI, P.P., DEIANA, G. & GALDENZI, S. 2013. Stratigraphic and structural features of the Sibillini Mountains (Umbria-Marche Apennines, Italy). *Italian Journal of Geosciences* **132**(3), 497–520.

RENARD, F., CANDELA, T. & BOUCHAUD, E. 2013. Constant dimensionality of fault roughness from the scale of micro-fractures to the scale of continents. *Geophysical Research Letters* **40**(1), 83–87.

SCHUSTER, A. 1898. On the investigation of hidden periodicities with application to a supposed 26 day period of meteorological phenomena. *Journal of Geophysical Research* **3**(1), 13.

Acknowledgments

مؤسسة قطر
Qatar Foundation

Additional references

BISTACCHI, A., GRIFFITH, W.A., SMITH, S.A.F., DI TORO, G., JONES, R.R. & NIELSEN, S. 2011. Fault Roughness at Seismogenic Depths from LIDAR and Photogrammetric Analysis. *Pure and Applied Geophysics* **168**(12), 2345–2363.

CANDELA, T., RENARD, F., BOUCHON, M., BROUSTE, A., MARSAN, D., SCHMITTBUHL, J. & VOISIN, C. 2009. Characterization of Fault Roughness at Various Scales: Implications of Three-Dimensional High Resolution Topography Measurements. *Pure and Applied Geophysics* **166**(10–11), 1817–1851.

HE, H., WEI, Z. & DENSMORE, A. 2016. Quantitative morphology of bedrock fault surfaces and identification of paleo-earthquakes. *Tectonophysics* **693**, 22–31.

MANDELBROT, B.B. 1985. Self-Affine Fractals and Fractal Dimension. *Physica Scripta* **32**(4), 257–260.

OLKOWICZ, M., DABROWSKI, M. & PLUYMAKERS, A. 2019. Focus stacking photogrammetry for micro-scale roughness reconstruction: a methodological study. *The Photogrammetric Record* **34**(March), 11–35.

SCHMITTBUHL, J., GENTIER, S. & ROUX, S. 1993. Field measurements of the roughness of fault surfaces. *Geophysical Research Letters* **20**(8), 639–641.

ZAMBRANO, M., PITTS, A.D., SALAMA, A., VOLATILI, T., GIORGIONI, M. & **TONDI, E.** 2019. Analysis of Fracture Roughness Control on Permeability Using SfM and Fluid Flow Simulations: Implications for Carbonate Reservoir Characterization. *Geofluids* **2019**, 1–19.